Supporting Information

Ni, S co-doped Cu dendrites decorated with core-shell architecture assisted by MOF and $Fe_{0.92}Co_{0.08}S$ nanoflakes on nanocellulose/graphene fibers for fabrication of flexible wire-type micro-supercapacitor

Leila Naderi, Saeed Shahrokhian*

Department of Chemistry, Sharif University of Technology, Tehran 11155-9516, Iran

*Corresponding author, Tel.: +98-21-66005718; Fax: +98-21-66002983

E-mail address: shahrokhian@sharif.edu

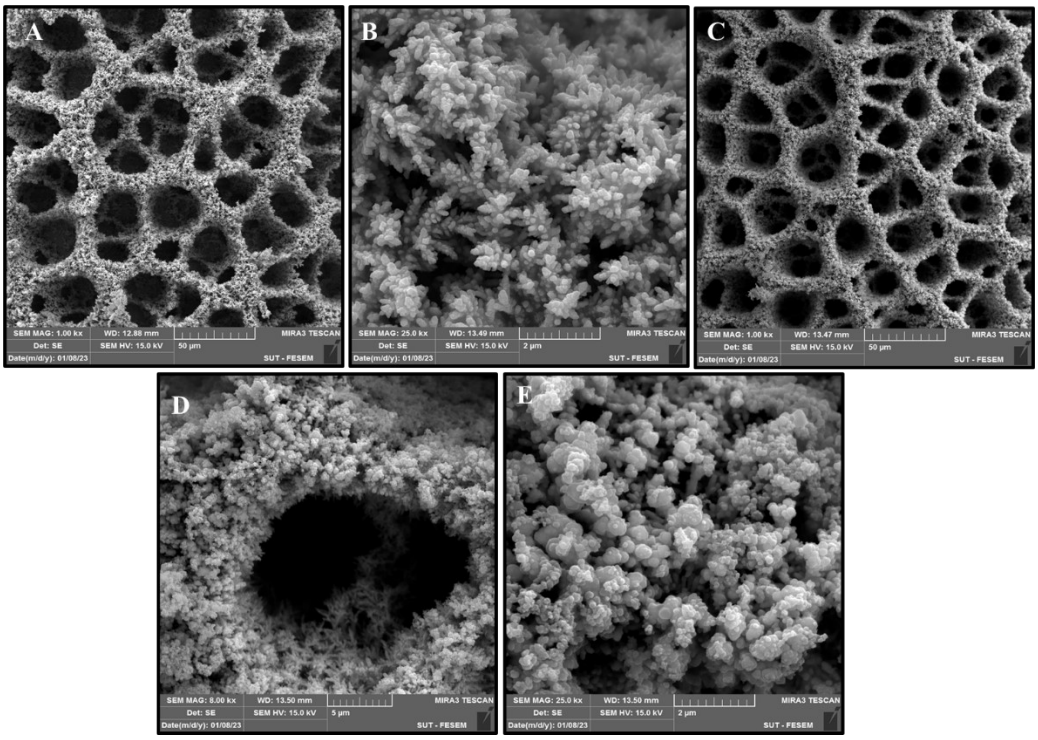

Fig. S1. FE-SEM images of the (A, B) Cu film@CW, (C-E) Ni,S-doped Cu@CW

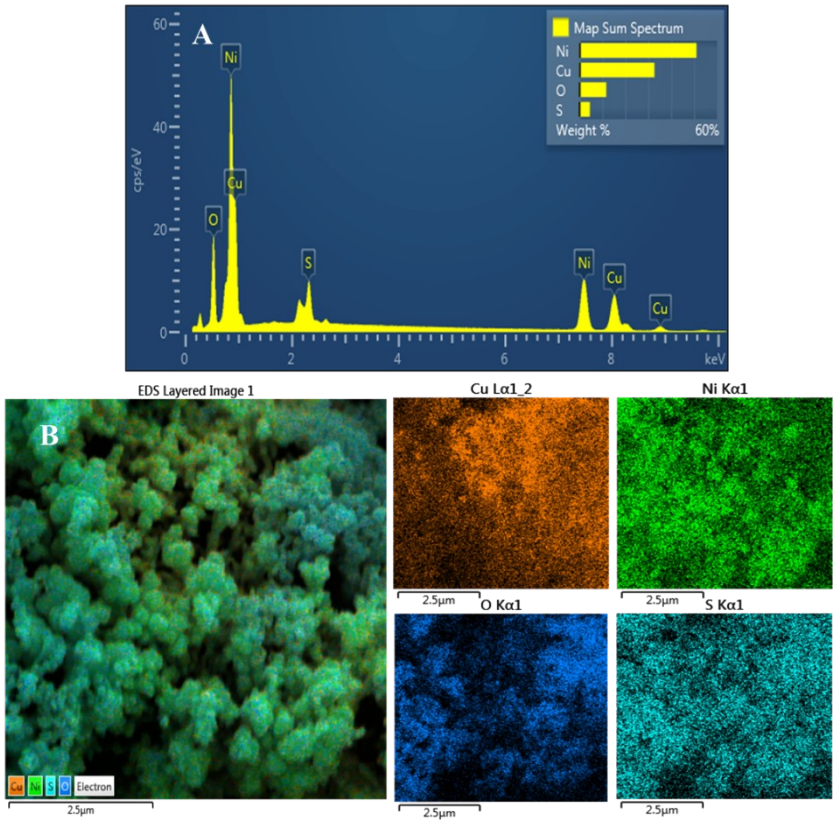

Fig. S2. (A) EDX spectra, (B) Elemental mapping of the Ni,S doped Cu@CW

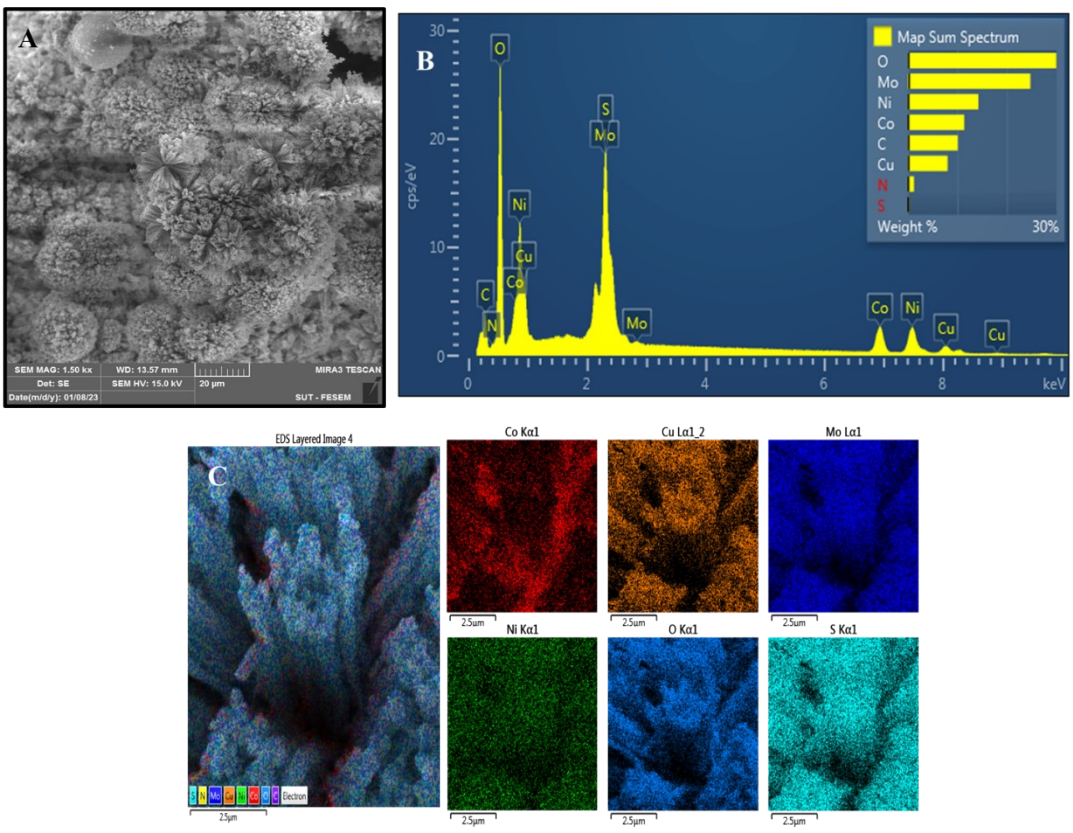

Fig. S3. (A) FESEM images, (B) EDX spectra, (C) elemental mapping of the NiMoCo-LTH/Ni,S-doped Cu@CW

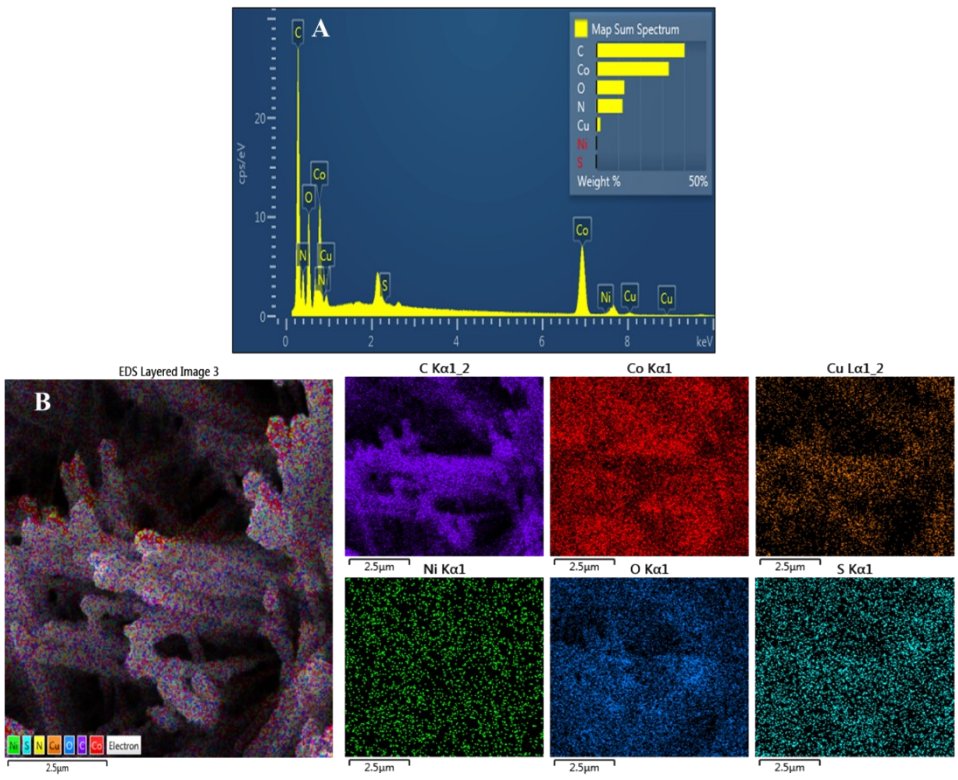

Fig. S4. (A) EDX spectra, (B) Elemental mapping of the ZIF-67@Ni,S-doped Cu@CW

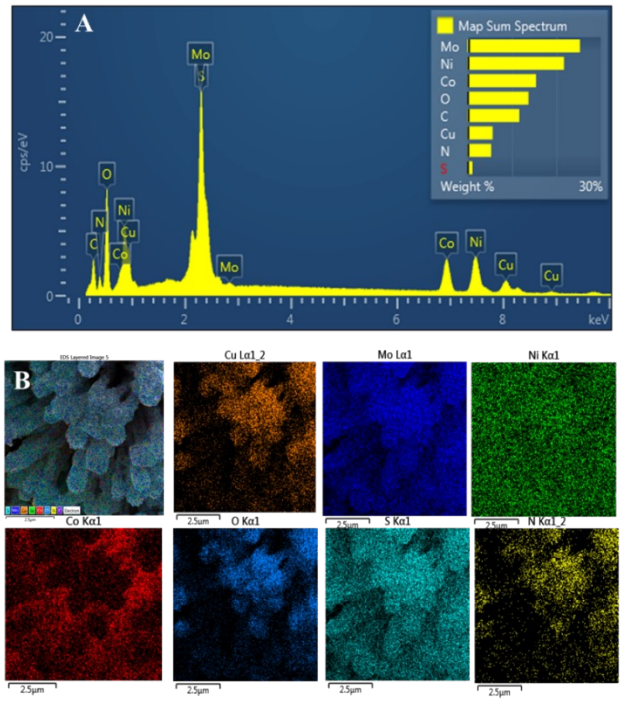

Fig. S5. (A) EDX spectra, (B) elemental mapping of the Ni_2Mo_3N-CoN/Ni,S-doped Cu@CW

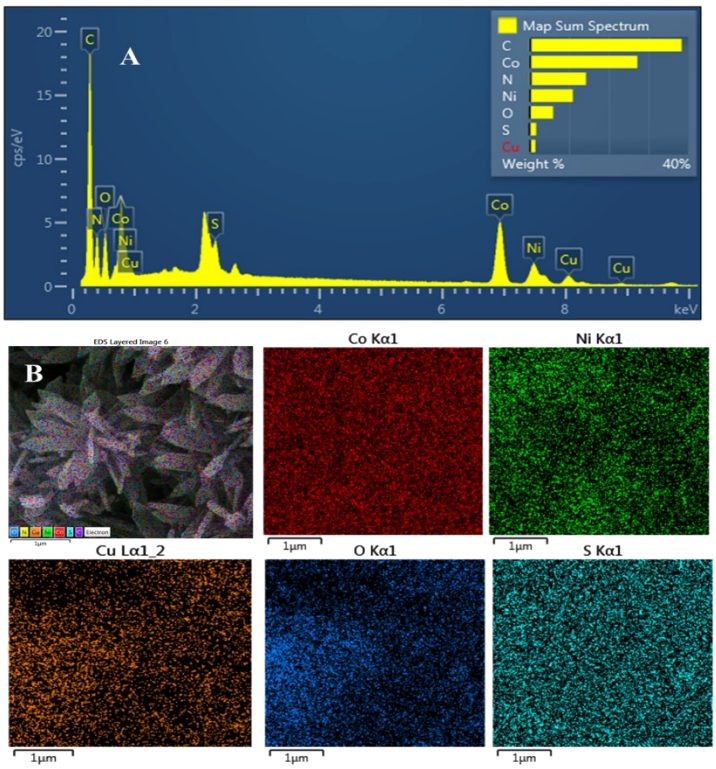

Fig. S6. (A) EDX spectra, (B) elemental mapping of the ZIF-Co leaf-like/Ni,S-doped Cu@CW

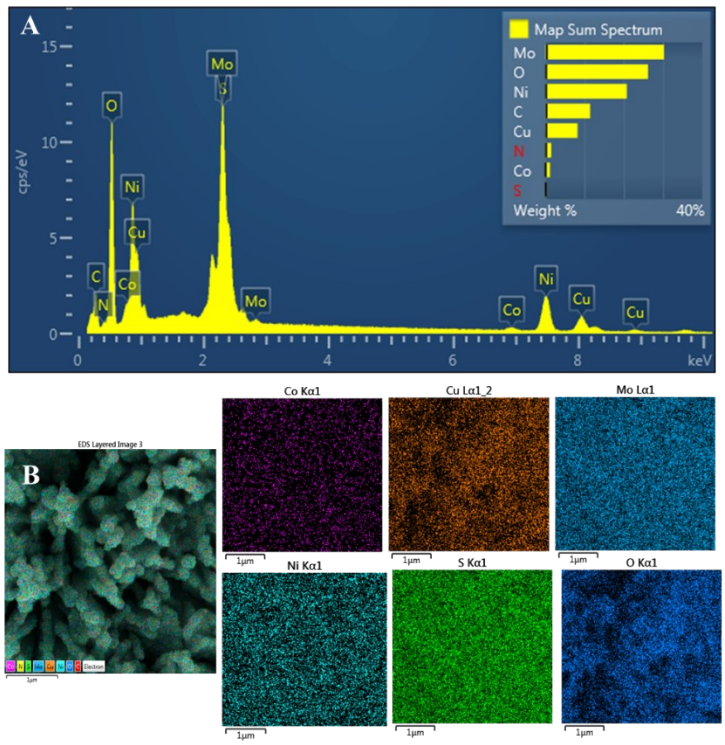

Fig. S7. (A) EDX spectra, (B) elemental mapping of the L-NiMoCo-LTH/Ni,S-doped Cu@CW

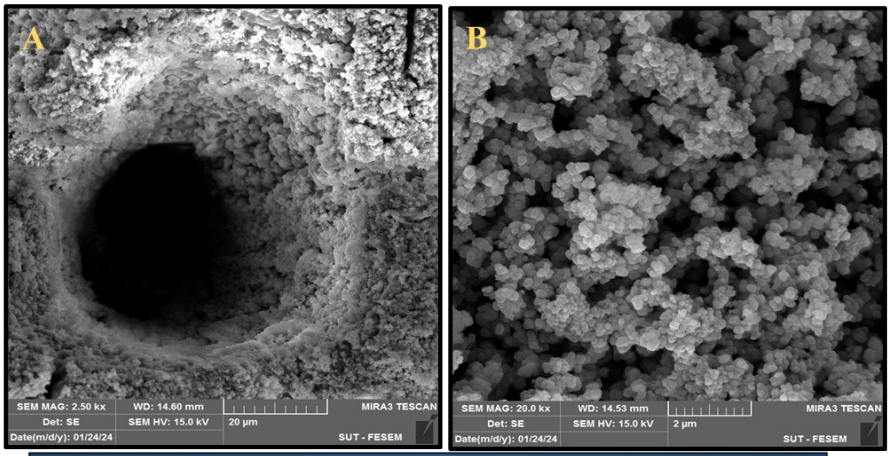
A
SEM MAG: 2.50 kx
WD: 14.60 mm
MIRA3 TESCAN
Det: SE
SEM HV: 15.0 kV
20 µm
Date(m/d/y): 01/24/24
SUT - FESEM
B
SEM MAG: 20.0 kx
WD: 14.53 mm
MIRA3 TESCAN
Det: SE
SEM HV: 15.0 kV
2 µm
Date(m/d/y): 01/24/24
SUT - FESEM

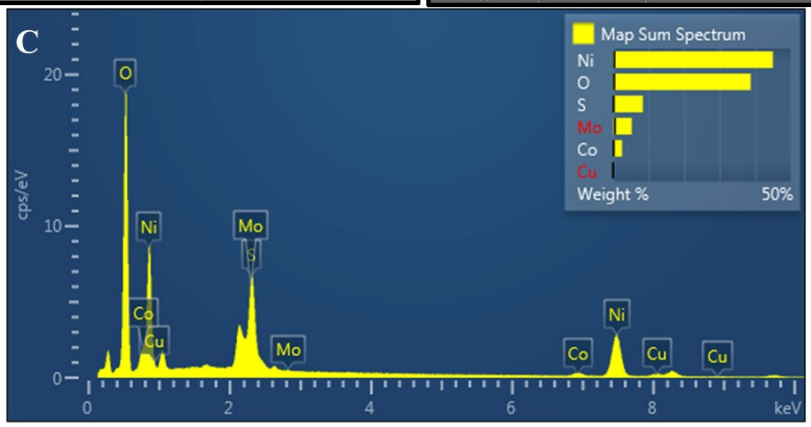
C
Map Sum Spectrum
Ni
O
S
Mo
Co
Cu
Weight %
50%
cps/eV
20
10
0
O
Ni
Mo
S
Co
Cu
Mo
Co
Ni
Cu
Cu
0
2
4
6
8
keV

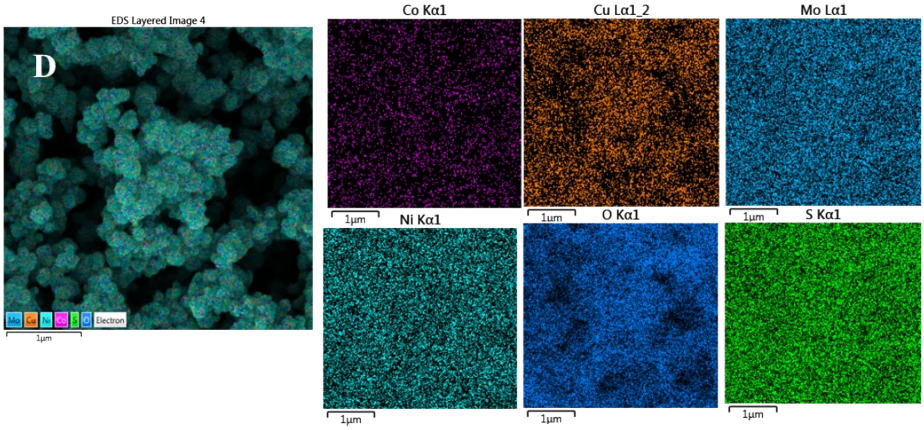
EDS Layered Image 4
D
Mo
Cu
Ni
Cu
S
O
Electron
1µm
Co Kα1
Cu Lα1_2
Mo Lα1
1µm
1µm
1µm
Ni Kα1
O Kα1
S Kα1
1µm
1µm
1µm

Fig. S8. (A, B) FE-SEM images, (C) EDX spectra, (D) elemental mapping of the E-NiMoCo-LTH/Ni,S-doped Cu@CW

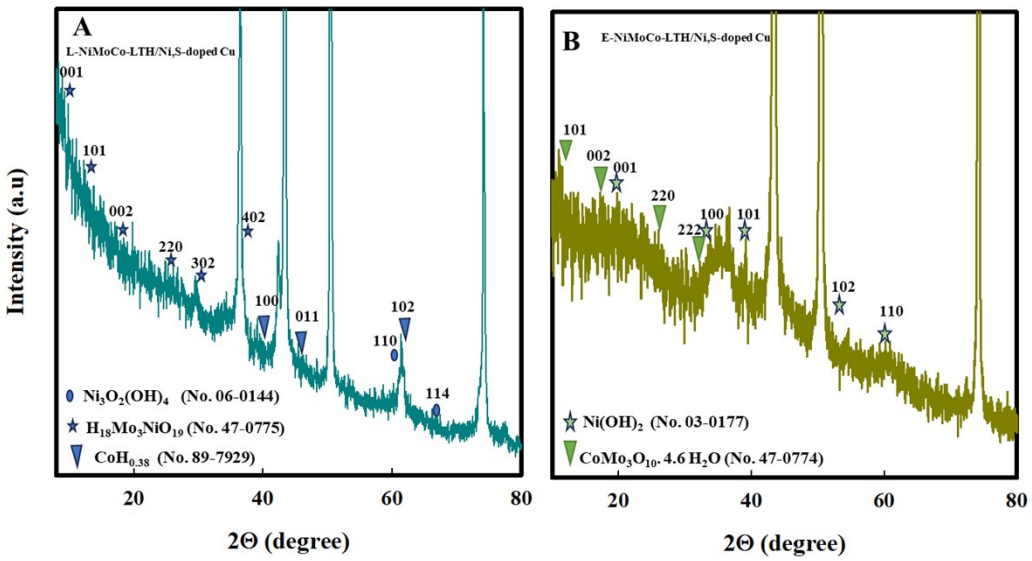

Fig. S9. XRD patterns of the (A) L-NiMoCo-LTH/Ni,S-doped Cu@CW, and (B) E-NiMoCo-LTH/Ni,S-doped Cu@CW

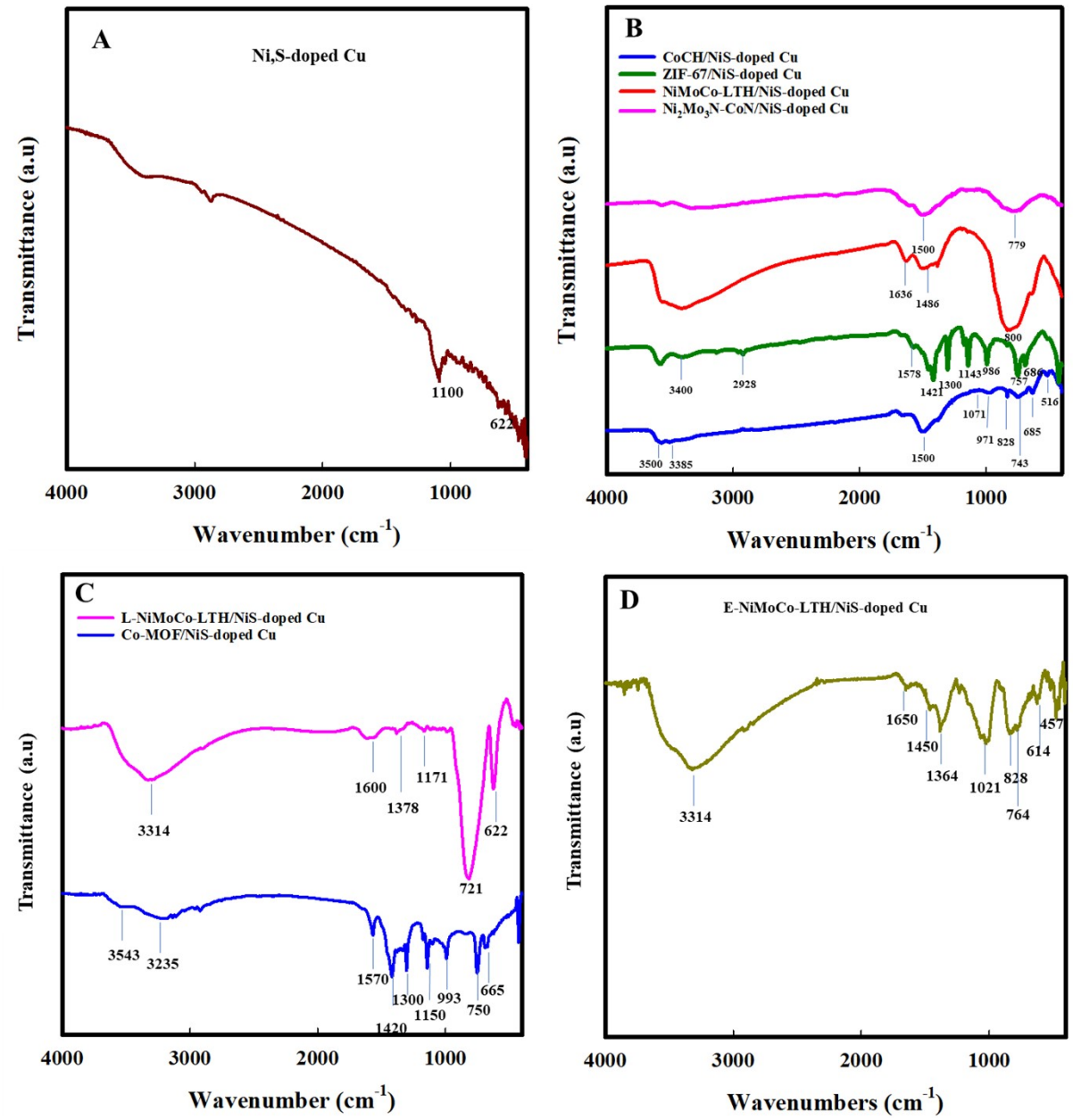

Fig. S10. FT-IR spectra of the (A) Ni,S-doped Cu, (B) CoCH/Ni,S-doped Cu, ZIF-67/Ni,S-doped Cu, NiMoCo-LTH/Ni,S-doped Cu, Ni_2Mo_3N-CoN/Ni,S-doped Cu, (C) ZIF-Co leaf-like/Ni,S-doped Cu, L-NiMoCo-LTH/Ni,S-doped Cu and (D) E-NiMoCo-LTH/Ni,S-doped Cu

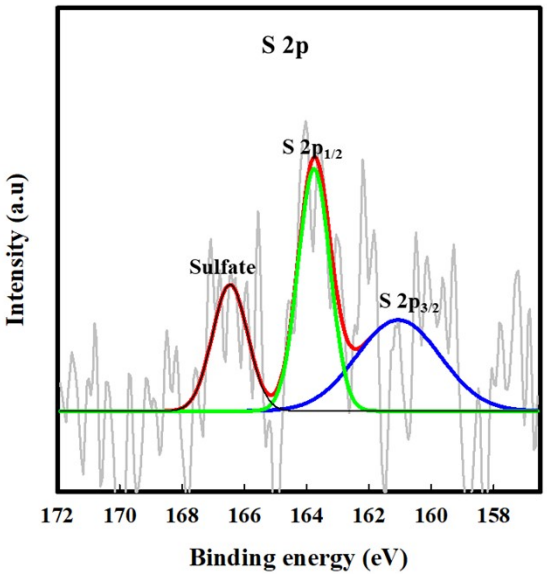

Fig. S11. XPS spectra of the S 2p

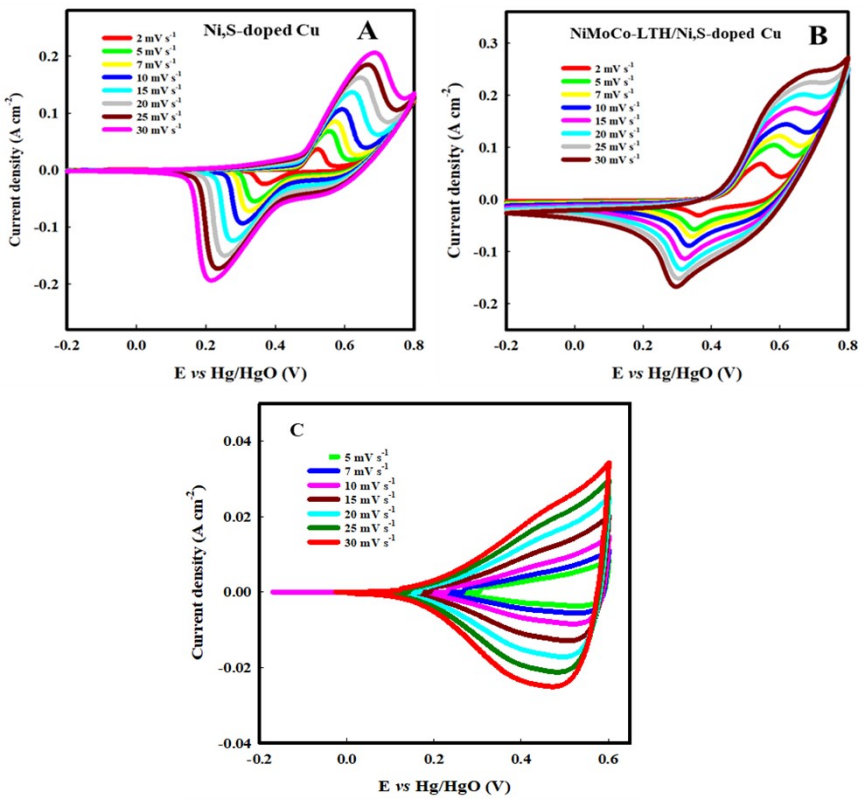

Fig. S12. CV curves of the (A) Ni,S-doped Cu@CW, (B) NiMoCo-LTH/Ni,S-doped Cu@CW and (C) Cu film at different scan rates

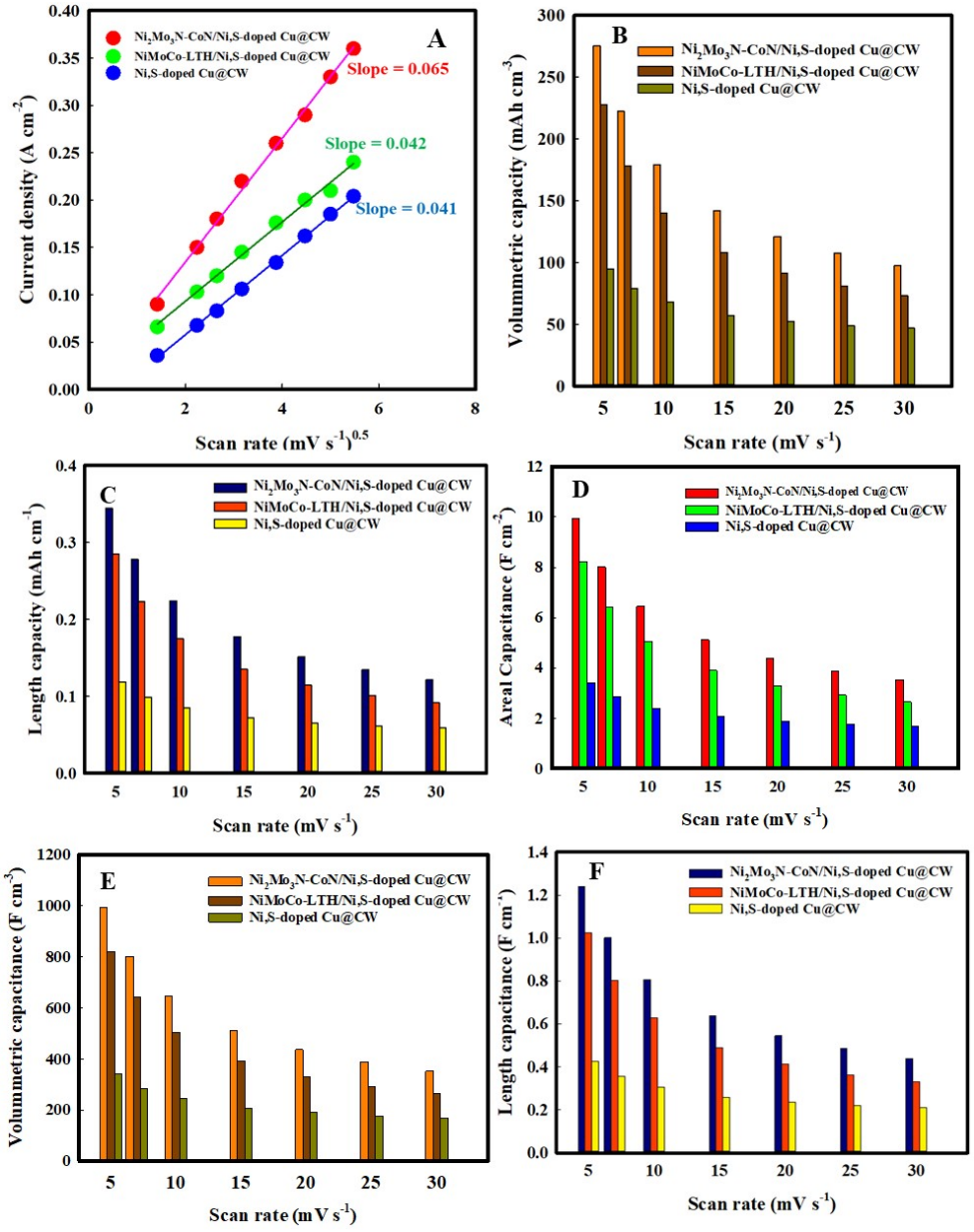

Fig. S13. (A) Plot of the current density as function of the scan rate square root, (B) Plot of the volumetric and (C) length capacities, (D) Areal, (E) volumetric and (F) length capacitance calculated from CV curves for the Ni,S-doped Cu/CW, NiMoCo-LTH/Ni,S-doped Cu@CW, Ni_2Mo_3N-CoN/Ni,S-doped Cu@CW microelectrodes at different scan rates.

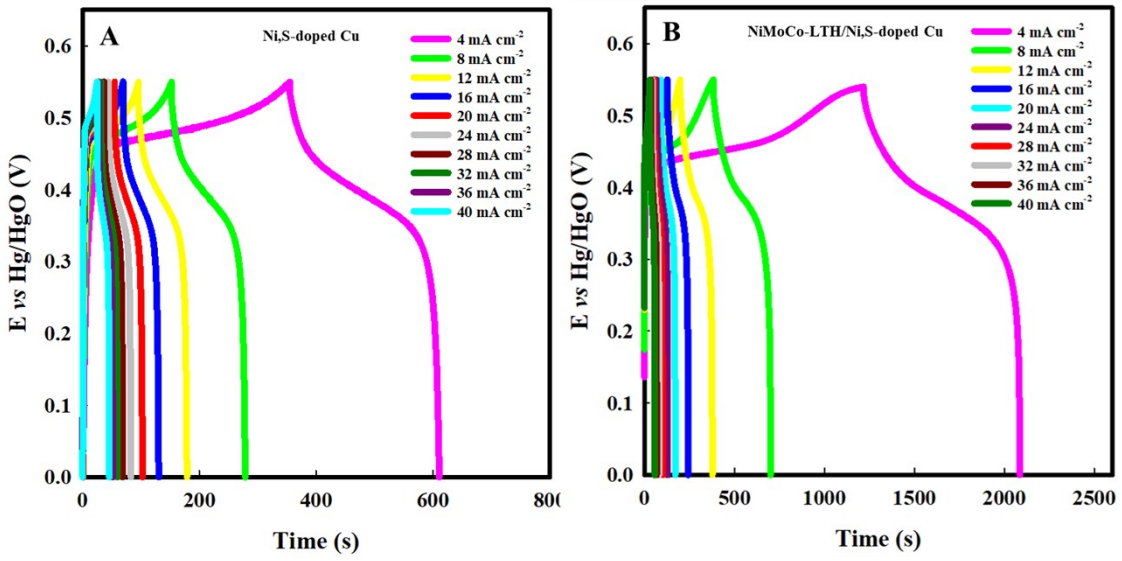

Fig. S14. GCD curves of the (A) Ni,S-doped Cu and (B) NiMoCo-LTH/Ni,S-doped Cu at different current densities

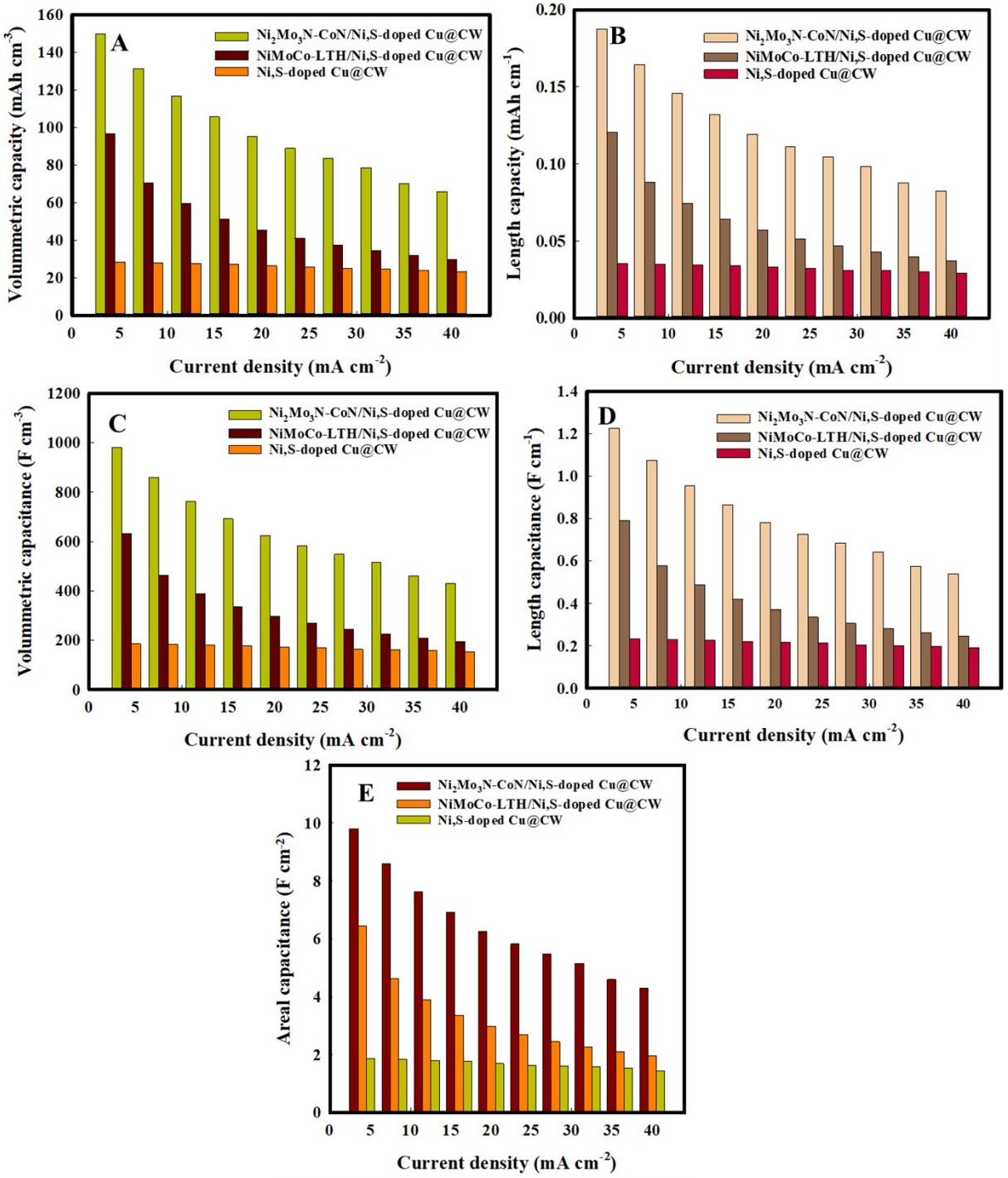

Fig. S15. Plot of the (A) volumetric, (B) length capacities and (C) volumetric, (D) length, (E) areal capacitances calculated from GCD curves for the Ni,S-doped Cu/CW, NiMoCo-LTH/Ni,S-doped Cu@CW, Ni_2Mo_3N-CoN/Ni,S-doped Cu@CW microelectrodes at different current densities.

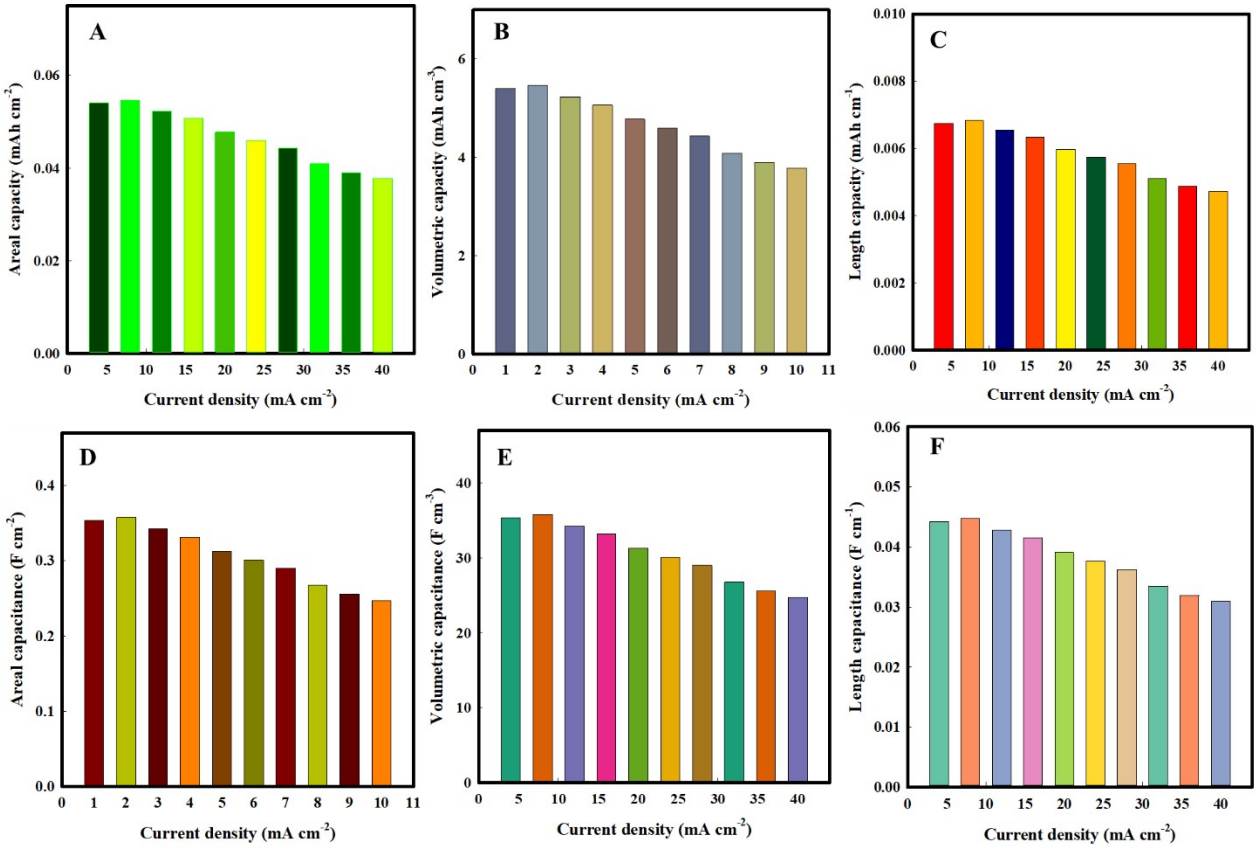

Fig. S16. Plot of the (A)Areal, (B) volumetric and (C) length capacities and (D) Areal, (E) volumetric and (F) length capacitances, calculated from GCD curves for the Cu film@CW microelectrode at different current densities.

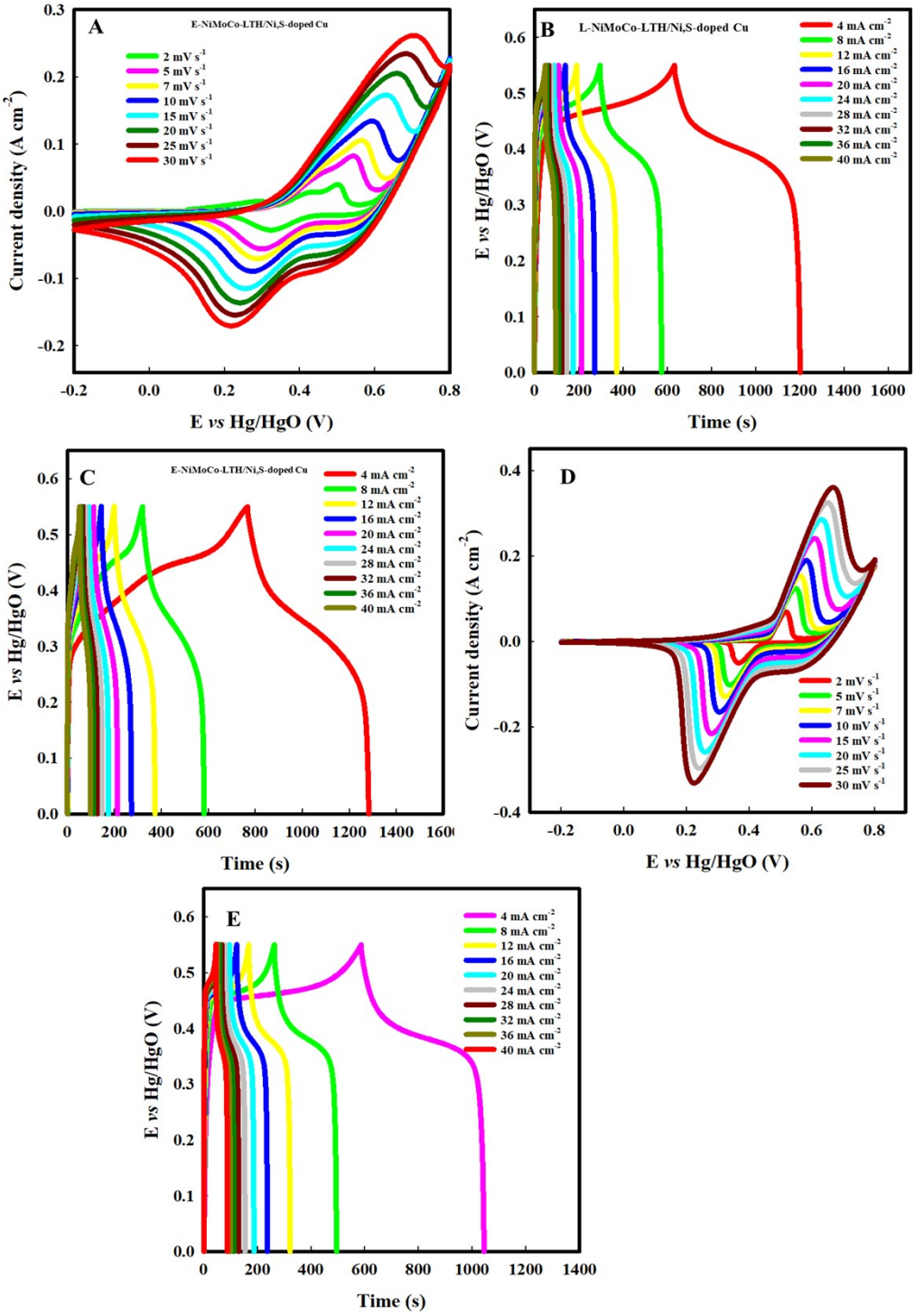

Fig. S17. (A) CV curves of the E-NiMoCo-LTH/Ni,S-doped Cu@CW at different scan rates, (B) GCD curves of the L-NiMoCo-LTH/Ni,S-doped Cu@CW at different current densities , (C) GCD curves of the E-NiMoCo-LTH/Ni,S-doped Cu@CW at different current densities, (A) CV curves of the NiMo-LDH/Ni,S-doped Cu@CW at different scan rates, (B) GCD curves of the NiMo-LDH/Ni,S-doped Cu@CW at different current densities

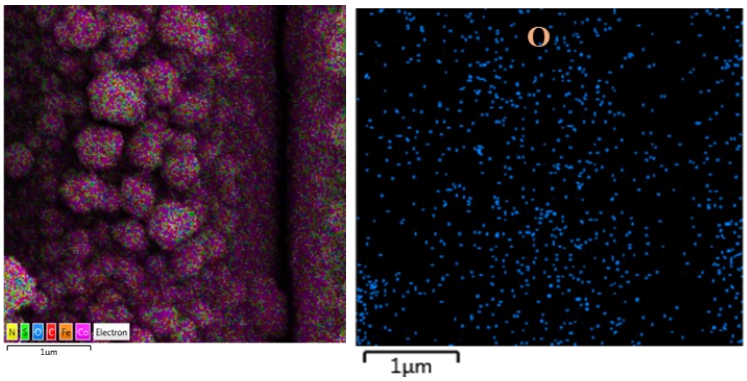

Fig. S18. Elemental mapping of the FeCoS/NCGH@CF

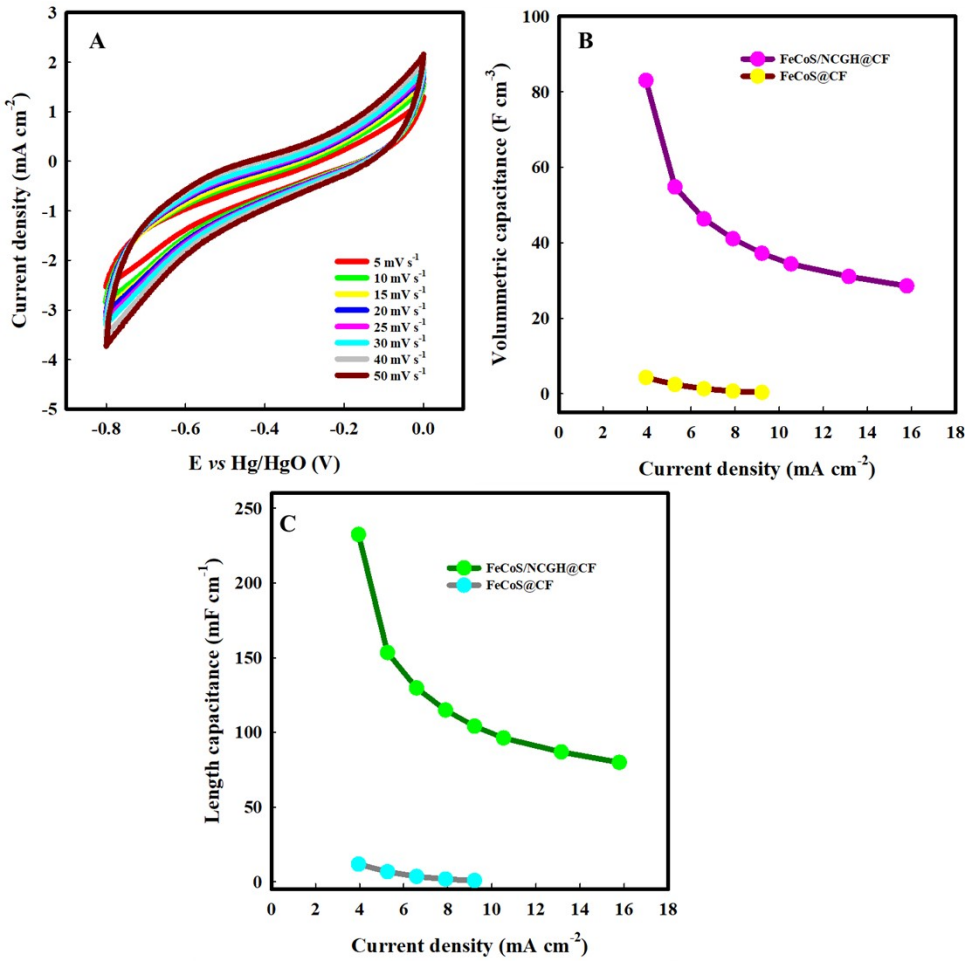

Fig. S19. (A) CV curves of the FeCoS@CF at different scan rates, (B) plot of the volumetric capacitance calculated from GCD curves for FeCoS@CF and FeCoS/GNCH at different current densities, (C) plot of the length capacitance calculated from GCD curves for FeCoS@CF and FeCoS/GNCH at different current densities.

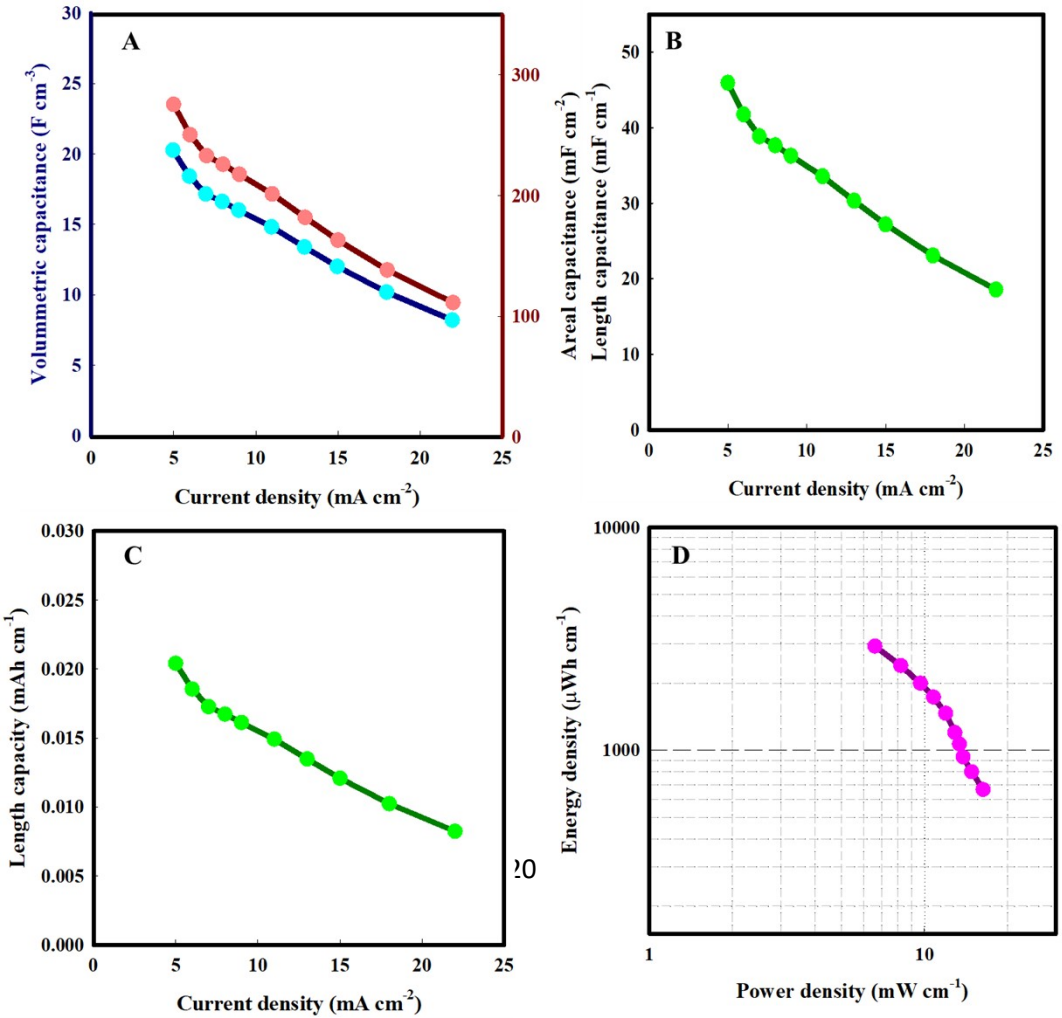

Fig. S20. Plot of the (A) Areal, volumetric capacities, and length (B) capacity and (C) capacitance calculated from GCD curves 1D microdevice at different current densities, (B) length Ragon plot for 1D microdevice

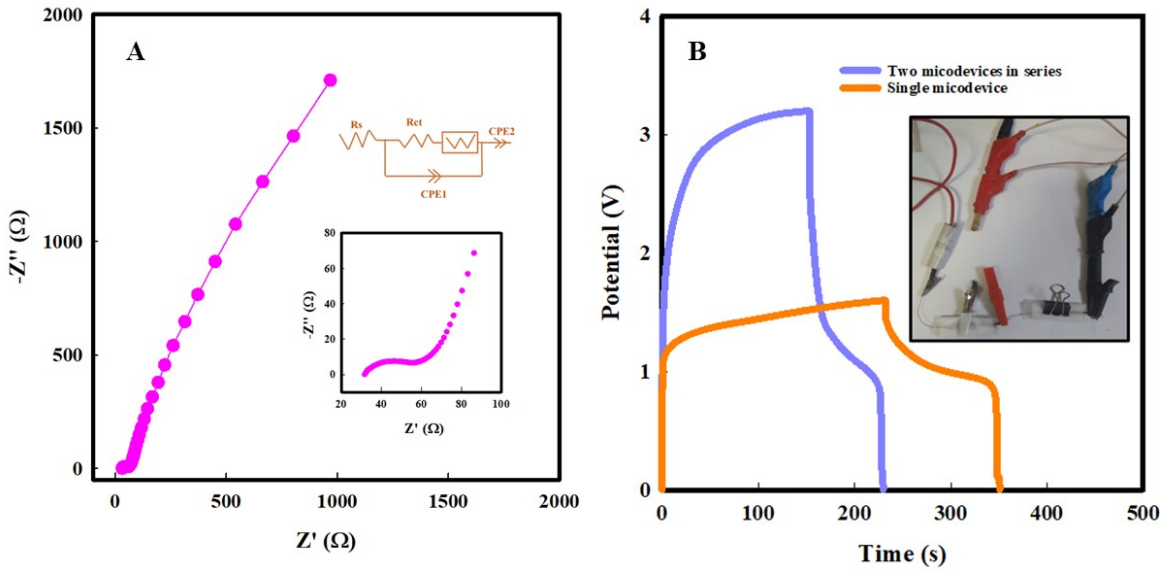

Fig. S21. (A) EIS spectra of the assembled microdevice, (B) GCD profiles of two micro-devices connected in series at 1.25 mA.

Electrode material	Areal capacity (capacitance)	Volumetric capacity (capacitance)	Length capacity (capacitance)
Ni,S-doped Cu	0.947 mAh cm^{-2} (3.41F cm^{-2})	94.74 mAh cm^{-3} (341.06 F cm^{-3})	0.118 mAh cm^{-1} (426.3 mF cm^{-1})
NiMo-LDH/Ni,S-doped Cu	1.34 mAh cm^{-2} (4.84 F cm^{-2})	134.4 mAh cm^{-3} (483.76 F cm^{-3})	0.168 mAh cm^{-1} (604.7 mF cm^{-1})
NiMoCo-LTH/Ni,S-doped Cu	2.279 mAh cm^{-2} (8.204 F cm^{-2})	227.9 mAh cm^{-3} (820.4 F cm^{-3})	0.285 mAh cm^{-1} (1025.5 mF cm^{-1})
L-NiMoCo-LTH/Ni,S-doped Cu	1.31 mAh cm^{-2} (4.72 F cm^{-2})	131.1 mAh cm^{-3} (472 F cm^{-3})	0.164 mAh cm^{-1} (590 mF cm^{-1})
E-NiMoCo-LTH/Ni,S-doped Cu	1.92 mAh cm^{-2} (6.916 F cm^{-2})	192.1 mAh cm^{-3} (691.6 F cm^{-3})	0.240 mAh cm^{-1} (864 mF cm^{-1})
Ni2Mo3N-CoN/Ni,S-doped Cu	2.755 mAh cm^{-2} (9.92 F cm^{-2})	275.5 mAh cm^{-3} (992 F cm^{-3})	0.344 mAh cm^{-1} (1240 mF cm^{-1})

Table S1. Areal, volumetric and length capacity and capacitance values of the different microelectrodes at scan rate of 5 mV s^{-1}

Table S2. Areal, volumetric and length capacity and capacitance values of the different microelectrodes at current density of 4 mA cm^{-2}

Electrode material	Areal capacity (capacitance)	Volumetric capacity (capacitance)	Length capacity (capacitance)
Ni,S-doped Cu	0.284 mAh cm^{-2} (1.86 F cm^{-2})	28.4 mAh cm^{-3} (185.89 F cm^{-3})	0.0355 mAh cm^{-1} (232.4 mF cm^{-1})
NiMo-LDH/Ni,S-doped Cu	0.508 mAh cm^{-2} (3.32 F cm^{-2})	50.8 mAh cm^{-3} (332.5 F cm^{-3})	0.063 mAh cm^{-1} (415.6 mF cm^{-1})
NiMoCo-LTH/Ni,S-doped Cu	0.966 mAh cm^{-2} (6.32 F cm^{-2})	96.6 mAh cm^{-3} (632.14 F cm^{-3})	0.121 mAh cm^{-1} (790.2 mF cm^{-1})
L-NiMoCo-LTH/Ni,S-doped Cu	0.631 mAh cm^{-2} (4.13 F cm^{-2})	63.1 mAh cm^{-3} (413.23 F cm^{-3})	0.079 mAh cm^{-1} (516.5 mF cm^{-1})
E-NiMoCo-LTH/Ni,S-doped Cu	0.573 mAh cm^{-2} (3.75 F cm^{-2})	57.33 mAh cm^{-3} (375.27 F cm^{-3})	0.0716 mAh cm^{-1} (469 mF cm^{-1})
Ni_2Mo_3N-CoN/Ni,S-doped Cu	1.5 mAh cm^{-2} (9.81 F cm^{-2})	149.92 mAh cm^{-3} (981.3 F cm^{-3})	0.187 mAh cm^{-1} (1230 mF cm^{-1})

Table S3. Performance comparison of the Ni_2Mo_3N-CoN/Ni,S-doped Cu@CW with other reports

Electrode materials	Current collectors	Current density	Specific capacitance	Ref
Ni_2Mo_3N-CoN/Ni,S-doped Cu	Cu wire	4 mA cm^{-2}	9.81 F cm^{-2} 981.3 F cm^{-3} 1.22 F cm^{-1}	This work
S-doped CoZnNi-OH/CuCoP	Cu wire	4 mA cm^{-2}	2.9 F cm^{-2} 290.1 F cm^{-3} 0.348 F cm^{-1}	1
$MnCo_2O_4$ @Co_3O_4	Ni foam (using binder)	1 mA cm^{-2}	3199.24 mF cm^{-2}	2

CuO/CF@ NiCoMn−OH	Cu foam	8 mA cm^{-2} 1 A g^{-1}	26.8 F cm^{-2} 2866 F g^{-1}	3
Ni-P@NMC-LDH	Ni foam	1 A g^{-1}	2980 F g^{-1}	4
NiCoMo oxide	Ni foam	1 A g^{-1}	3.31 F cm^{-2}	5
NiMo-LDH	Ni foam	4 mA cm^{-2}	4.4 F cm^{-2}	6
$CuO@NiMoO_4$	Cu foam	3 mA cm^{-2}	3.9 F cm^{-2}	7
$Cu_3N@NiCo–N/Cu$	Cu foam	1 mA cm^{-2}	8.49 F cm^{-2}	8
Co_9S_8	Ni foam	1 A g^{-1}	369.1 mAh g^{-1}	9
Cu_xO NW@CoS_2	Cu foam	1 mA cm^{-2}	2.46 mAh cm^{-3}	10
$MnCo_2O_4$/porous Ni/Ni	Cu wire	2 mA cm^{-2}	1.798 F cm^{-2}	11
3D-NiCo2S4	Ni wire	0.2 mA cm^{-1}	199.74 F cm^{-3} 98 mF cm^{-1} 1.248 F cm^{-2}	12
3D-NiCoO4	Ni wire	2.5 mA	38.84 F cm^{-3}	13

Table S4. the comparative of the electrochemical properties of electrodes based on fiber substrates and similar electroactive material for supercapacitor

Supercapacitor	Specific capacitance	Current density	Voltage	Maximum energy density	Maximum power density	Stability	Ref
Ni_2Mo_3N-CoN/Ni,S-doped Cu@CW//FeCoS/ GNCH@CF	275.6 mF cm^{-2} 20.3 F cm^{-3}	5 mA cm^{-2}	1.6 V	98 µWh cm^{-2} 7.2 mWh cm^{-3} 16.3 µWh cm^{-1}	17.6 mW cm^{-2} 1294 mW cm^{-3} 2933 µW cm^{-1}	94% after 5000 cycles At 10 mA cm^{-2}	**This work**
CuO/CF@NiCoMn−OH//AC	19.3 F g^{-1}	2 A g^{-1}	1.5 V	37.28 W h kg^{-1}	At 170 W kg^{-1}	62.5% even at 3000 cycles at 8 A g-1	3
Ni-Co-N/GP||GOP Substrate: graphene paper	4.24 F/cm^3 42.3 mF/cm^2	0.5 mA/cm^2	1.6 V	4.78 mWh cm^{-3}	1.26 W/cm^3	89% after 8000 cycles at 5 mA cm-2	14
0.075 Mo-NiCo-LDH@C//RGO Substrate: CC	235.1 C g-1	1 A g-1	1.6 V	52.2 Wh kg^{-1}	32.2 Wh kg^{-1}	84.2 % after 10000 cycles at 10 A g-1	15
Cu3N@NiCo–N/Cu//rGO Substrate: Cu foam	351.3 mF cm- 2	2 mA cm-2	1.6 V	124.9 µWh cm^{-2} 12.49 mWh cm^{-3}	8 mW cm^{-2} 0.8 W cm^{-3}	After 8000 cycles at 20 mA cm^{-2} 86.68%	8
NF/Ni-P@NMC-LDH//AC Substrate: NF	202.67 F g-1	0.8 A g-1	1.8 V	91.2 Wh kg^{-1}	1812.3 W·kg^{-1}	86.97 % after 5000 cycles at 3 A g^{-1}	4
$MnCo_2O_4$@Co_3O_4/ /AC Substrate: NF	1338 C cm^{-2} 148.7 C g^{-1}	2.5 mA cm^{-2}	1.5 V	31 Wh kg^{-1}	3326.6 Wkg^{-1}	101.23% after 8000 cycles at 130 mA cm^{-2}	2
Co3S4@NiO//AC Substrate: powder pasted on NF	164.80 F g^{-1}	1 A g^{-1}	1.55 V	54.99 Wh kg^{-1}	19.10 kW kg^{-1}	86.1% after 10,000 cycles at 5 A g-1	16
NiCoMoO-P//N-rGO Substrate: NF	109.1F g- 1	0.5 A g-1	1.6 V	45.3 Wh Kg^{-1}	4000 W Kg^{-1}	60% after 2000 Cycles at 1 A g-1	17
$CoNi_2S_4$/E–NZP //rGO (solid state) Substrate: CW and CF	241 mF cm^{-2} 18.54 F cm^{-3}	4 mA cm^{-2}	1.8 V	108.4 µWh cm^{-2} 8.34 mWh cm^{-3}	9280 µW cm^{-2} 716.9 mW cm^{-3}	88.89% after 5000 cycles at 5.6 mA cm-2	18
CoZnNiS@CNTs/rGO //carbon spheres integrated graphene	185.1 F cm^{-3}	1.5 A g^{-1}	1.6 V	65.2 W h L^{-1}	at 1308 W L^{-1}	90.6% after 10000 cycles	19
CoVSe/NiCuSe@CW//PPy/RGO@CF	351.7 mF cm^{-2} 56.73 F cm^{-3}	4.8 mA cm^{-2}	1.6 V	111.4 µWh cm^{-2} 20.17 mWh cm^{-3}	12900 µW cm^{-2} 2081.14 mW cm^{-3}	96.7% after 5000 cycles at 6.4 mA cm^{-2}	20
Symmetric Cu@Ni/porous Ni/ MnCo2O4	54.8 mF cm^{-2} –	0.18 mA cm^{-2}	1.3 V	4.8 µWh cm^{-2}	1040 µW cm^{-2}	-	11
NiCo2S4 //N-rGO	120 mF cm^{-2} 19.57 F cm^{-3}	0.2 mA	1.4 V	32.67 µWh cm^{-2} 5.33 mWh cm^{-3}	5352.92 µW cm^{-2} 855.69 mW cm^{-3}	92% after 1000 cycles at 3 mA	12

References

[1] L. Naderi, S. Shahrokhian. Wire-type flexible micro-supercapacitor based on MOF-assisted sulfide nano-arrays on dendritic CuCoP and V2O5-polypyrrole/nanocellulose hydrogel. *Chem. Eng. J.* 476 (2023) 146764.

[2] J-J. Zhou, X. Han, K. Tao, Q. Li, Y-L. Li, Ch. Chen, L. Han, Shish-kebab type MnCo2O4@Co3O4 nanoneedle arrays derived from MnCo-LDH@ZIF-67 for high-performance supercapacitors and efficient oxygen evolution reaction, Chem. Eng. J. 354 (2018) 875–884.

[3] L. Lei, X. Zhang, Y. Su, Sh. Wu, J. Shen, Metal−Organic Framework (MOF)-Assisted Construction of Core−Shell Nanoflower-like CuO/CF@NiCoMn−OH for High-Performance Supercapacitor, Energy Fuels 2021, 35, 8387−8395

[4] J. Wang, Y. Zou, C. Xiang, F. Xu, L. Sun, Ternary NiMoCo-layered double hydroxides grown on chemically plated Ni–P alloyed nickel foam for high-performance supercapacitors, Journal of Energy Storage 58 (2023) 106388.

[5] H. Huang, X. Wei, G. Wei, F. Yan, L. Yan, Y. Han, Sh. Xu, X. Liang, W. Zhou, J. Guo, Construction of vertically aligned Ni-Co-Mo hybrid oxides nanosheet array for high-performance hybrid supercapacitors, J. Alloys Compd. 899 (2022) 163267.

[6] Y. B. Chen, J. J. You, Y. H. Chen, L. A. Ma, H. X. Chen, Z. H. Wei, X. Y. Ye, L. Zhang, Low-crystalline nickel hydroxide nanosheets embedded with NiMoO4 nanoparticles on nickel foam for high-performance supercapacitor applications. CrystEngComm 24 (2022) 5238-5250.

[7] D. Yu, Z. Zhang, Y. Teng, Y. Meng, Y. Wu, X. Liu, Y. Hua, X. Zhao, X. Liu, Fabrication of CuO@NiMoO4 core-shell nanowire arrays on copper foam and their application in high-performance all-solid-state asymmetric supercapacitors. J. Power Sources 440 (2019) 227164.

[8] Z. Hu, Y. Miao, H. Chen, L. Ding, J. Qi, F. Wei, Q. Meng, B. Xiao, X. Xue, Q. Yin, Y. Li, Y. Sui, X. Feng, W. Zhang, P. Cao, J. Liu, Ultrathin nickel cobalt nitride nanoflowers embedded in Cu3N porous nanorod arrays for ultrahigh capacitance energy storage, J. Power Sources 536 (2022) 231485.

[9] Zh. Peng, H. Zou, W. Yang, Zh. Feng, Sh. Chen. Hierarchical porous Co9S8 nanowire arrays derived from zeolitic imidazolate framework on Ni foam for button-type asymmetric supercapacitor. J. Energy Storage 40 (2021) 102697.

[10] G.P. Ojha, A. Muthurasu, A. P. Tiwari, B. Pant, K. Chhetri, T. Mukhiya, B. Dahal, M. Lee, M. Park, H-Y. Kim, Vapor solid phase grown hierarchical Cu_xO NWs integrated MOFs-derived CoS2 electrode for high-performance asymmetric supercapacitors and the oxygen evolution reaction. Chem. Eng. J. 399 (2020) 125532

[11] Y. Ji, J. Xie, J. Wu, Y. Yang, X.Z. Fua, R. Sun, C.P. Wong, Hierarchical nanothorns MnCo2O4 grown on porous/dense Ni bi-layers coated Cu wire current collectors for high performance flexible solid-state fiber supercapacitors, J. Power Sources, 2018, 393 54–61.

[12] B. Saravanakumar, S.S. Jayaseelan, M.K. Seo, H.Y. Kim, B.S. Kim, NiCo2S4 nanosheet-decorated 3D, porous Ni film@Ni wire electrode materials for all solid-state asymmetric supercapacitor applications, Nanoscale, 2017, 9, 18819-18834.

[13] A. Ramadoss, K.-N. Kang, H.-J. Ahn, S.-I. Kim, S.-T. Ryu, J.-H. Jang, Realization of high-performance flexible wire supercapacitors based on 3-dimensional NiCo2O4/Ni fibers, J. Mater. Chem. A 4 (2016) 4718–4727.

[14] F. Liu, L. Zeng, Y. Chen, R. Zhang, R. Yang, J. Pang, L. Ding, H. Liua, W. Zhou, Ni-Co-N hybrid porous nanosheets on graphene paper for flexible and editable asymmetric all-solid-state supercapacitors, Nano Energy 61 (2019) 18–26

[15] L. Xu, Y. Li, M. Li, N. Yu, W. Wang, F. Wei, J. Qi, Y. Sui, L. Li, L. Zhang, Mo-doped NiCo-LDH nanoflower derived from ZIF-67 nanosheet arrays for high-performance supercapacitors, Journal of Energy Storage 77 (2024) 109781.

[16] Sh. Hou, Y. Lian, Y. Bai, Q. Zhou, Ch. Ban, Zh. Wang, J. Zhao, H. Zhang, Hollow dodecahedral Co3S4@NiO derived from ZIF-67 for supercapacitor, Electrochimica Acta 341 (2020) 136053.

[17] H. Huang, C. Li, F. Yan, F. Yuan, X. Liang, W. Zhou, J. Guo, Bi-functional Ni-Co-Mo hybrid oxide/phosphide nanoarrays grown on Ni foam with enhanced charge storage and oxygen evolution reaction performance, Applied Surface Science 623 (2023) 157079.

[18] S. Shahrokhian, L. Naderi, High-Performance, Flexible, All-Solid-State Wire-Shaped Asymmetric Micro-Supercapacitors Based on Three Dimensional CoNi 2S 4 Nanosheets Decorated−Nanoporous Ni−Zn−P Film/Cu Wire, J. Phys. Chem. C 2019, 123, 21353−21366.

[19] Y. Liu, Na Xin, Q. Yang, W. Shi, 3D CNTs/graphene network conductive substrate supported MOFs derived CoZnNiS nanosheet arrays for ultra-high volumetric/gravimetric energy density hybrid supercapacitor, Journal of Colloid and Interface Science 583 (2021) 288–298.

[20] L. Naderi, Saeed Shahrokhian, Cobalt vanadium chalcogenide microspheres decorated with dendrite-like fiber nanostructures for flexible wire-typed energy conversion and storage microdevices, Nanoscale, 2022, 14, 9150.